Nonlinear Voltage Velocity–Torque Feedback Controller Applied to High–Torque Hybrid Stepper Servomotor ⋆

Javier Ollervides, Ariel González, Marco Arjona and Víctor Santibáñez.

Instituto Tecnológico de la Laguna, Blvd. Revolución y Cuauhtémoc, Torreón, Coah., 27000, Mexico (e-mail: jollervi@itlalaguna.edu.mx)

Abstract: High torque hybrid stepper motors *HSM* concern to a family of synchronous brushless AC (*BLAC)* servomotors with become a popular choice when implementing high–precision controllers for mechatronic systems. This paper takes the main features of the complete electromechanical model of a *BLAC–HSM* system defined in modern literature, to propose a nonlinear feedback velocity–torque controller named *Voltage Velocity–Torque Feedback Controller*. Finally, the experimental system response show that regulation and tracking control are satisfied, i.e., the velocity error signal is bounded around the origin.

1. INTRODUCTION

The high torque hybrid stepper motors named by us *BLAC–HSM* are extended actual alternative for many high performance motion control task. Typical applications include robotic systems, mobile robots, computer numeric control (*CNC*) machines, and servopositioning of mechatronic systems (Khorrami et al. [2003])). The *BLAC–HSM* is a doubly salient machine which incorporates a permanent magnet in the rotor shaft as described in (Acarnley [1984]). The *HSM* complicates the control problem by coupling multi-input nonlinear dynamics into the overall electromechanical system dynamics, it is possible to develop an accurate dynamic model. In presented work, we apply the nonlinear sinusoidal conmutation to design of a velocity–torque tracking controller for the *BLAC–HSM* driving a mechanical load. In this paper some experimental results will be presented concerned to evaluation of velocity–torque controller proposed by us. The model *BLAC–HSM* is applied without transformation for the nonlinear controller development.

The main idea of controller design consider that the motor is a source torque and thus design a desired torque signal to ensure that de load follows the desired velocity trajectory. Since the developed motor torque is a function of rotor position and the electrical winding currents, we utilize a simple sinusoidal commutation strategy to tracking the desired torque signal as a set of desired current trajectories. The voltage control inputs are then formulated to force the electrical winding currents to follow the desired current trajectories. That is the electrical dynamics are taken into account through the current tracking objective, and hence the velocity tracking control objective is embedded inside the current tracking objective. Therefore, if the voltage control input can be designed to guarantee that the actual currents track the desired currents then the load velocity will follow the desired velocity trajectory, just as it is mentioned in the reference (Dawson et al. [1998]).

The implementation is based on PC Pentium IV (master μP) linked with PCI Multi–Q *slavecard* data acquisition system (*PCI–DAS*) manufactured by Quanser. Linear power amplifier designed by us, to drive *BLAC–HSM*, and conditioning integrated electronic circuits for shunt current measurements.

The resulting performance advantages of closed loop controller over stepping technique, compensate for the additional circuit cost and complexity.

2. SYSTEM MODEL

The dynamics of the load position for a two–phase hybrid magnet stepper servo motor can be described by a set of differential equations as in (Blauch et al. [1993]) and (Kuo et al. [2002]). Such a representation allows for a distinct segregation of the mechanical and electrical components of the system dynamics. The dynamics are decomposed into one mechanical subsystem and two electrical subsystems that are coupled by the torque transmission and back–emf terms. The coupling between the subsystems is an integral part of motor operation. The dynamics of mechanical subsystem for a position dependent–load (see Figure 2) actuated by a permanent magnet stepper motor are assumed to be of the form (Spong et al. [1989]), (Zribi et al. [1991]) as it is mentioned in the reference (Dawson et al. [1998]).

$$M\ddot{q} + B\dot{q} + Nsin(q) + K_D sin(4N_r q) = K_m \sum_{j=1}^{2} -sin(x_j) I_j \tag{1}$$

where $q(t)$, $\dot{q}(t)$, and $\ddot{q}(t)$ represent the load position, velocity, and acceleration, respectively. The constant parameter M denotes de mechanical inertia of the rotor shaft and the connected load, B represent the viscous damping or

⋆ This work was partially supported by DGEST and CONACyT–Mexico.

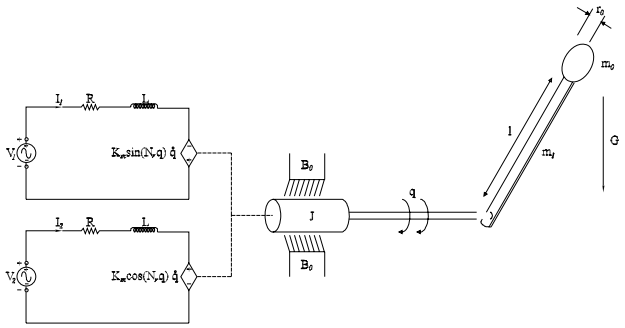

Fig. 1. Schematic Diagram of *BLAC–HSM* Servoactuator with Load System.

viscous friction coefficient, N denotes the constant lumped load term, and the constant K_m represents the torque coefficient which characterizes the In English electromechanical conversion of electrical winding currents to torque. The term $K_D sin(4N_r q)$ is used to model the detente torque, and K_D is usually referred to as the detente torque constant. The terms $\sum_{j=1}^{2} -sin(x_j)I_j$ can be considered as torque inputs originating in the electrical subsystems that generating the electrical torque of electric machine, I_j denotes the particular phase current signal, and x_j is given by (as described in reference (Dawson et al. [1998]))

$$x_j = N_r q - (j-1)\frac{\pi}{2} \tag{2}$$

in which N_r accounts for the number of theet on the rotor.

The current dynamics for the two electrical subsystems are described by ([12])

$$L\dot{I}_j = v_j - RI_j + K_m \dot{q} sin(x_j), \quad j = 1, 2 \tag{3}$$

where v_j is the voltage input to a particular phase. The constant electrical parameters R and L desribe de winding resistance and inductance, respectively. The back–emf term $K_m \dot{q} sin(x_j)$ can be considered as inherent feedback for the mechanical subsystem. The electrical subsystems described by the parameters R, L, and K_m are assumed to be the same for each of the two phases. The interconnection of the subsystems is illustrated in Figure 1 where the system inputs are the voltages v_j, and the output is the load velocity $\dot{q}$.

3. CONTROLLER DESIGN

The controller design is based on micro–stepping closed loop technique. Micro–stepping open loop is technique by which the position resolution of the motor may be increased by allowing the phase currents to take on a large number of possible current values, there by increasing the number of equilibrium states. Usually, the current values are chosen such that the step lengths are integer fractions of the full step length. Micro–stepping results in reduced vibrations, noise and permits smoother motion compared to full– or half–stepping (as described in reference (Khorrami et al. [2003])). Micro–stepping open loop technique considers the electrical developed form of torque expression

$$\tau = K_m(-I_1 sin(N_r q) + I_2 cos(N_r q)) \tag{4}$$

where the phase currents are defined by

$$I_1 = I_m \cos(\phi) \tag{5}$$

$$I_2 = -I_m \sin(\phi) \tag{6}$$

where the phase currents I_m is a fixed constant, usually referred to as the motor current and ϕ is a controlled variable. Using (5), (4) reduces to

$$\tau = K_m I_m sin(N_r q - \phi) \tag{7}$$

The equilibrium points of torque equation are the positions where the torque generated by the motor is zero:

$$N_r q - \phi = n\pi, \quad n = 0, \pm 1, \pm 2, ... \tag{8}$$

By controlling the motor angle ϕ, the equilibrium position of the motor may be changed, and this is the principle of micro–stepping. For a motion for one microstep, the value of ϕ_j is incremented discontinuously by $\delta\phi$ (on real–time controller driver), producing a pulsating torque that is dependly of DAC resolution in the electronic driver. For motion of several microsteps, the motor angle is incremented in rapid succession until the desired set point is reached (as described in reference (Khorrami et al. [2003])). The speed of the motor is proportional to the rate of change of ϕ since change of 2π corresponds to motion over one tooth pitch,

$$\frac{\Delta\phi}{\Delta t} \equiv \omega = N_r \dot{q} \tag{9}$$

where ω is the electrical speed of the rotor shaft.

Unlike the brushed DC servomotor where the commutation of the electrical windings done by a mechanical commutator (*i.e.*, the brushes), commutation of the *BLAC–HSM* must be incorporated into the controller design (as previously mentioned). In order to generate the appropriate current in each electrical phase (Dawson et al. [1998]), we propose the following continuous, differentiable commutation strategy for the *BLAC–HSM*

$$I_{d1} = -\tau_d sin(\phi) \tag{10}$$

$$I_{d2} = \tau_d cos(\phi) \tag{11}$$

where I_{dj} corresponding to desired current for micro–stepping closed loop technique and τ_d is the desired torque designed to force the load to track the desired velocity trajectory.

Given full state measurements (i.e. q, $\dot{q}$, I_1 and I_2), the control objective is to develop load velocity tracking controller for the electromechanical dynamics of (1) through (3). To begin the development, we define the load velocity tracking error

$$\dot{e} = \dot{q}_d - \dot{q} \tag{12}$$

where $\dot{q}_d(t)$ represents the desired load velocity trajectory and $\dot{q}(t)$ was defined in (1). We will assume that $\dot{q}_d(t)$ is a continuous function fully differentiable of time.

The controller that we implemented, contains a high gain *PI+P* velocity outer loop controller, that operates in conjunction with a high gain *PI* torque–current feedback inner loop controller. The velocity controller algorithm

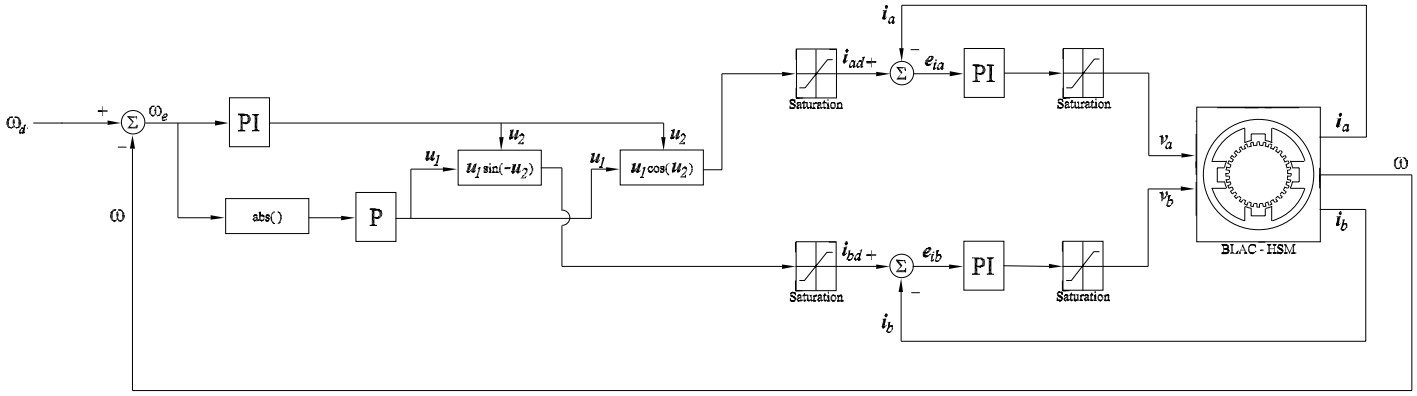

Fig. 2. Block Diagram of Voltage Velocity–Torque Controller System.

feeds the phase and amplitude of a sinusoidal commutation of (10) (see Figure 2), the controller is described by

$$\tau_d = k_{pa}\dot{e} \tag{13}$$

$$\phi = k_{pv}\dot{e} + k_{iv}\int \dot{e}\ dt. \tag{14}$$

Considering the structure of the electromechanical system given by (1) through (3), we are only free o specify the two phase voltages, v_1 and v_2. In other words, the mechanical subsystem error dynamics lack true current (torque) level control inputs. For this reason, we add a high gain PI torque–current feedback inner loop controller described by

$$v_j = k_{pcj}\eta_j + k_{ij}\int \eta_j\ dt. \tag{15}$$

where η_j represents the current tracking error of electrical subsystem dynamics of the form

$$\eta_j = I_{dj} - I_j \tag{16}$$

4. SIMULATION RESULTS

The efficacy of the proposed controller is demonstrated using simulation for $BLAC$–HSM servoactuator connected with a single–link manipulator, with the following parameters: $L = 3[mH]$, $R = 0.7\ [\Omega]$, $k_m = 0.025[V-s]$, $K_D = 0.0[N-m]$, $M = 2.6835\times10^{-4}$ and $B = 0.632[\frac{kg-m}{s}]$. The desired rotor velocity tracking trajectory $\dot{q}_d(t)$ (see Figure 8) is a sinusoidal function defined by

$$\dot{q}_d(t) = 2\pi\sin(2\pi f_d t)\ \left[\frac{rad}{s}\right] \tag{17}$$

were $f_d = 0.2\ Hz$ is the frequency of velocity tracking reference. Initial conditions for all states are zero. The simulations are shown for a period of 10 $[s]$. The following

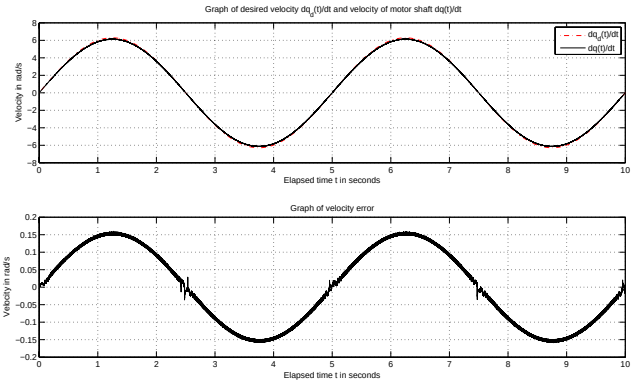

Fig. 3. Simulation of Velocity Response and Tracking Error of $BLAC$–HSM Servoactuator with Load System.

control gains were utilized in the proposed rotor velocity tracking controller of (13), (14) and (15)

$$K_{pa} = 30,\ K_{pv} = 20,\ K_{iv} = 2000 \tag{18}$$

$$K_{pc_j} = 10,\ K_{ic_j} = 500 \tag{19}$$

The simulation results are shown in Figure 3. It is seen that the rotor shaft velocity track the desired trajectory with maximum error of $0.15\frac{rad}{s}$ approximately. The simulation results of phase currents are shown in Figure 4 and phase voltages are shown in Figure 5. Due to symmetry, the various phase voltages and currents exhibit similar time responses, except for peak values. The dynamics observed in the phase voltages and phase currents exhibits amplitude modulation (torque compensation), and frequency modulation (phase velocity compensation), that which was of being expected, as shown in Figures 4 and 5.

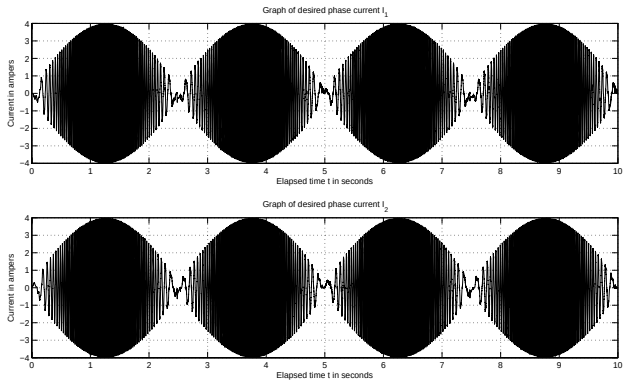

Fig. 4. Simulation of Current Response (Phase One and Two) of *BLAC–HSM* Servoactuator with Load System.

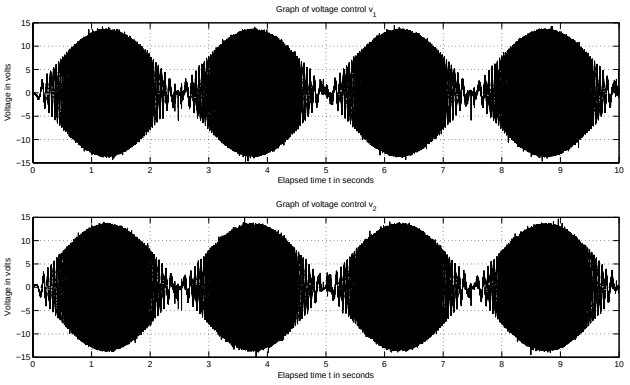

Fig. 5. Simulation of Voltage Control (Phase One and Two) of *BLAC–HSM* Servoactuator with Load System.

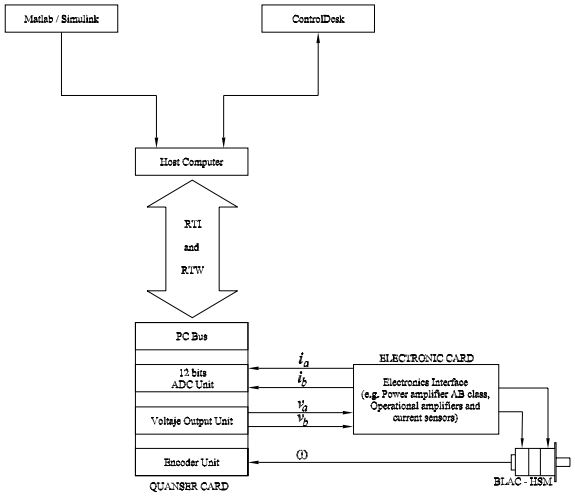

Fig. 6. Experimental Setup.

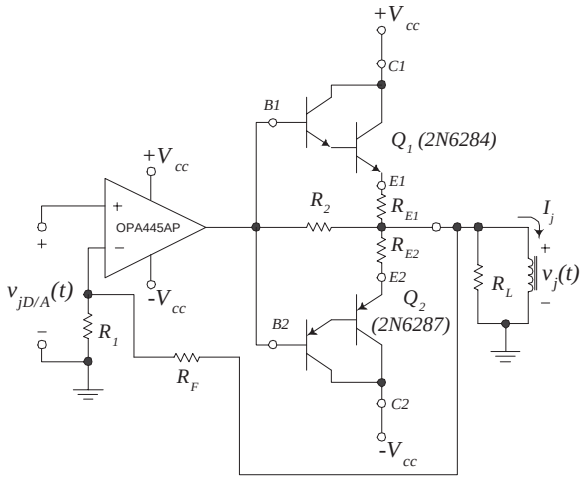

Fig. 7. Class AB Power Servoamplifier applied to stator windings.

5. EXPERIMENTAL SYSTEM RESPONSE

The laboratory controller setup is presented in Figure 6. Experiments were conducted on a two-phase *HSM–BLAC* servoactuator (Anaheim 34Y High–Torque Series) powered by two linear voltage class AB feedback amplifier designed by us, (based on a servoamplifier circuit exposed in reference (Burr–Brown–TI [2000]), with operational amplifier OPA445AP, BJT 2N6284–NPN, and 2N6287–PNP transistor devices, mounted in house heating) as see in Figure 7. Two magneto–resistive shunt current sensors (F.W. Bell, Model NT–5) were used to measure the stator phase currents. A Windows XP based real–time MatLab–Simulink environment serves as the user interface required to implement de control algorithm. The control algorithm was depicted in Simulink block diagram environment, that it compiles block–diagram to *C++ programming language*, and executes algorithm controller on a *Pentium IV processor*. The sampling frequency was selected to be 5 $[KHz]$. The *MultiQ board* (8 A/D, 8 D/A, and 6 encoder channels) manufactured by Quanser Consulting was used as the hardware interface to output the two phase voltages to the stepper motor and read in the two phase currents. External optical encoder (Fabricated by US Digital Corp.) was mounted in the rotor shaft, equipped with 10000 counts/rev, whose signal is read in via the *MultiQ board* to obtain rotor position measurement. To obtain rotor velocity measurement, a backwards difference algorithm is then applied to the rotor signal with the resulting signal being passed through a second order digital filter.

In the experiment, the desired rotor velocity trajectory $\dot{q}_d(t)$ (see Figure 8) was selected as follows

$$\dot{q}_d(t) = 2\pi \sin(2\pi f_d t) \ \left[\frac{rad}{s}\right] \tag{20}$$

were $f_d = 0.2\ Hz$ is the frequency of velocity tracking reference. Initial conditions for all states are zero. The simulations are shown for a period of 10 $[s]$.

The selection of the controller gains of (13), (14) and (15) was based on our past experience with motor control algorithms along with numerous trial and errors runs. Admittedly the tuning of a controller without proper

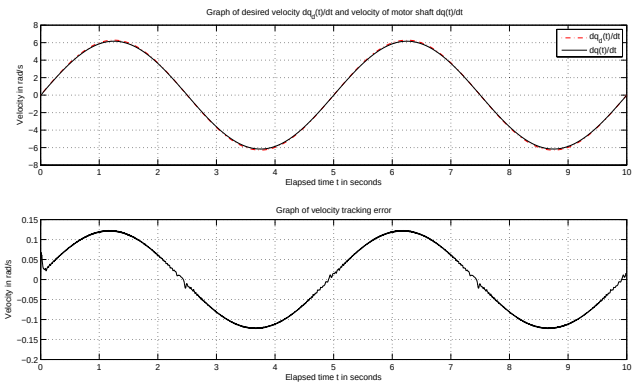

Fig. 8. Experimental Velocity Response and Tracking Error of *BLAC–HSM* Servoactuator with Load System.

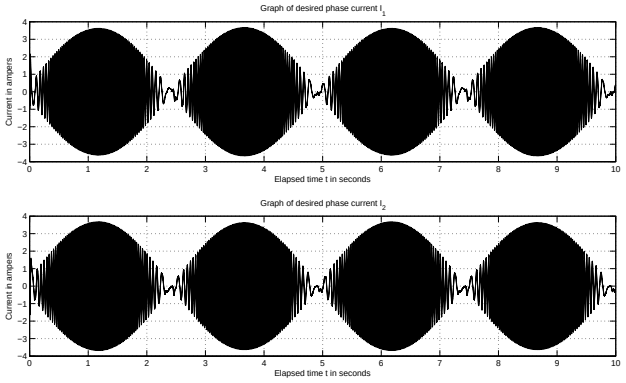

Fig. 9. Experimental Current Response (Phase One and Two) of *BLAC–HSM* Servoactuator with Load System.

guidelines is a bit tedious; however, we currently are not aware of any established procedures which can be used to tune the controller gains of a nonlinear control algorithm similar to that of the proposed approach (as mentioned in (Behal et al. [2000])).

The best performance was found by using the following control gains

$$K_{pa} = 30,\ K_{pv} = 20,\ K_{iv} = 2500 \tag{21}$$

$$K_{pc_j} = 20,\ K_{ic_j} = 1000 \tag{22}$$

The resulting position velocity tracking error is given in Figure 8 which indicates that the best steady state tracking error is approximately within $\pm 0.12[\frac{rad}{s}]$. The dynamics observed in the phase voltages and phase currents exhibits amplitude modulation (torque compensation), and frequency modulation (phase velocity compensation), that which was of being expected, as shown in Figures 9 and 10, this results correspond to simulation system response except for small variations in peak values.

6. CONCLUSION

Nowadays, *BLAC–HSM* servomotors are of interest since they are commonly used in several applications of high–precision position control.

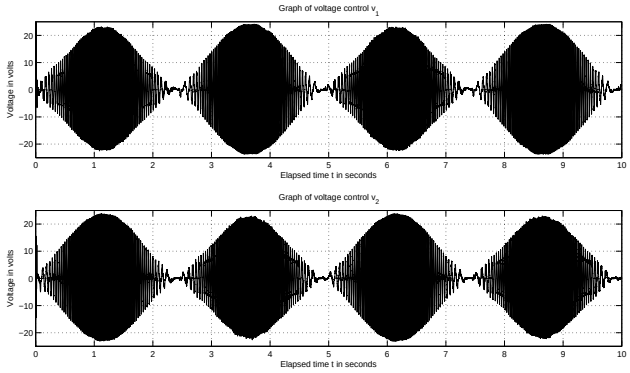

Fig. 10. Experimental Voltage Control (Phase One and Two) of *BLAC–HSM* Servoactuator with Load System.

This paper has recalled both the derivation of the complete electromechanical model of a *BLAC–HSM* servomotor, and presented a sensor control algorithm for the full–order model of the hybrid stepper motor actuating a mechanical subsystem that achieves sinusoidal rotor velocity tracking utilizing stator current and rotor shaft velocity measurements. At the end, simulations were carried out and compared with experimental results, showing a good performance.

REFERENCES

P. P. Acarnley Stepping Motors: A guide to Modern Theory and Practice. 2nd ed. Stevenage, U.K.: Peregrinus, 1984.

A. Behal, M. Feemster, D. Dawson, and A. Mangal. Sensorless Rotor Velocity Tracking Control of the Permanent Magnet Stepper Motor. *Proceedings of the 2000 IEEE International Conference Control Applications*, Anchorage, Alaska, USA, September 2000.

A. Blauch, M. Bodson, and J. Chiasson. High–Speed Parameter Estimation of Step Motors. *IEEE Transactions on Control Systems Technology*, Vol. 1, No. 4, pp. 270–279, Dec. 1993.

Burr–Brown of Texas Instruments. High Voltage FET-Input Operational Amplifier. Burr–Brown for Texas Instruments Inc., Data Sheet SBOS156B, 2008 (in `http://www.burr-brown.com`, `http://www.ti.com`).

D. Dawson, J. Hu and T.C. Burg. *Nonlinear Control of Electric Machinery*. Marcel Dekker, 1998.

F. Khorrami, P. krishnamurty, and H. Melkote. *Modeling and Adaptive Nonlinear Control of Electric Motors*. Springer-Verlag Berlin Heidelberg, 2003.

P.C. Krause, O. Wasynczuk, and S. D. Sudhoff. *Analysis of Electric Machinery and Drive Systems*. Wiley-Interscience, 2002.

B. Kuo, and J. Tal. *Incremental Motion Control, Step Motors and Control Systems*, Vol. II, SRL Publishing, Champaign, IL, 1979.

M. Spong and M. Vidyasagar. *Robot Dynamics and Control*. Jhon Wiley and Sons, Inc., 1989.

M. Zribi, and J. Chiasson. *Position Control of PM Stepper Motor by Exact Linearization. IEEE Transactions on Automatic Control*, Vol. 36, No. 5, pp. 620–625, May. 1991.